Global Energy Interconnection 9 (2026) 51–67

KeAi
CHINESE ROOTS
GLOBAL IMPACT

Global Energy Interconnection
Development and Cooperation Organization

Global Energy Interconnection

Contents lists available at ScienceDirect
journal homepage: www.elsevier.com/locate/gloei

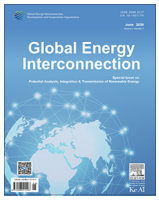


# Bi-level optimization of configurations and scheduling for the multi-microgrid system (MMS) considering shared hybrid electric-hydrogen energy storage service

Lu Li [a,b], Xulong Zhou [a], Shilong Chen [a,*], Guihong Bi [a], Zeliang Zhu [a], Yurui Fan [c]

[a] Faculty of Electrical Engineering, Kunming University of Science and Technology, Kunming 650500, PR China
[b] College of Engineering, Design and Physical Sciences, Brunel University of London, London UB8 3PH, UK
[c] Department of Civil and Environmental Engineering, Brunel University of London, London UB8 3PH, UK

Received 17 March 2025; revised 3 July 2025; accepted 19 September 2025

**Abstract**

Shared energy storage helps lower user investment costs and enhances energy efficiency, which is considered a pivotal driver in accelerating the green transition of energy sectors. In view of the increasing demand for hydrogen, this paper proposes a bi-level optimization of configurations and scheduling for combined cooling, heating, and power (CCHP) microgrid systems considering shared hybrid electric-hydrogen energy storage service. The upper-level model addresses the capacity allocation problem of energy storage stations, while the lower-level model optimizes the operational strategies for the multi-microgrid system(MMS). To resolve the complexity of the coupled bi-level problem, Karush-Kuhn-Tucker (KKT) conditions and the Big-M method are applied to reformulate it into a solvable mixed-integer linear programming (MILP) model, compatible with CPLEX. The economic viability and rationality of the proposed approach are verified through comparisons of three cases. Numerical results show that the proposed approach reduces user annual costs by 20.15% compared to MMS without additional energy storage equipment and achieves 100% renewable absorption. For operators, it yields 5.71 M CNY annual profit with 3.02-year payback. Compared to MMS with electricity sharing, it further cuts user costs by 3.84%, boosts operator profit by 60.71%, and shortens payback by 15.88%.

*Keywords:* Shared energy storage; Combined cooling, heating and power (CCHP); Hybrid electric-hydrogen energy; MMS; Karush-Kuhn-Tucker (KKT); Big-M

## 0 Introduction

Greenhouse gas emissions, especially carbon dioxide, account for 80% of total emissions due to human activity [1]. This directly contributes to the frequency of extreme weather events. Concomitant problems include rising global temperatures [2] and depletion of environmental resources [3]. To mitigate the potential environmental damage caused by climate change as much as possible, countries across the world have formally adopted, announced, or are considering net-zero emission goals in alignment with the Paris Agreement [4]. In 2020, China announced an expansion of its nationally determined contribution, aiming to achieve net-zero carbon dioxide emissions by 2060 [5].

The CCHP system is an energy-efficient and environmentally friendly system capable of delivering cooling, heating, and electricity simultaneously [6]. By introducing decoupling equipment into the traditional CCHP system, a

Peer review under the responsibility of Global Energy Interconnection Group Co. Ltd.
* Corresponding author.
*E-mail addresses:* 103586871@qq.com (L. Li), 2284778358@qq.com (X. Zhou), chenshilong3@163.com (S. Chen), KM_BGH@163.com (G. Bi), zhuzeliang99@163.com (Z. Zhu), yurui.fan@brunel.ac.uk (Y. Fan).

https://doi.org/10.1016/j.gloei.2025.09.001

CCHP microgrid can be established [7]. It can promote green energy production, improve energy efficiency [8], while reducing carbon dioxide emissions [9]. The implementation of CCHP microgrids contributes significantly to the achievement of "carbon neutrality".

Research on CCHP microgrids has already yielded some results. Reference [10] integrated a Power-to-Gas (P2G) device into a CCHP microgrid and applied a distributed robust optimization approach to address energy dispatch issues. The results showed that this method improves stability and economy. Reference [11] proposed a new multi-timescale dynamic robust optimal scheduling approach, significantly lower the operating expenses of CCHP microgrids and enhance the robustness of their cooperative operation. Reference [12] proposed an optimized scheduling framework for integrating adiabatic compressed air energy storage and CCHP microgrids, considering temperature dynamics. A pilot project conducted in China demonstrated that the system's operating costs were reduced by 13.7% compared to previous levels.

A substantial portion of research on CCHP microgrids emphasizes integrating advanced technologies or renewable energy sources, alongside developing innovative models and optimization methods. However, there is limited focus on the economic feasibility and practical implementation of these technologies, particularly within complex system configurations. At the same time, renewable energy is volatile and intermittent due to weather factors [13]. These studies do not perform well when dealing with uncertain renewable energy outputs. Microgrid systems require integrated energy storage equipment to manage the volatility of renewable energy [14]. However, the extensive and widespread deployment of energy storage equipment faces problems such as high costs, technical difficulties, and imperfect market mechanisms.

To tackle the problems mentioned above, some scholars have suggested new models of energy storage sharing. Reference [15] proposes a novel energy trading market equilibrium model that integrates peer-to-peer trading mechanisms with energy storage sharing and implements this model for residential consumers. Reference [16] extended the energy sharing model into direct and buffer sharing, developed a day-ahead stochastic planning model to assist energy sharers' decision-making. Reference [17] introduced another way of sharing, cloud energy storage (CES), which reduces the cost by exploiting consumer complementarities and economies of scale. Results for residential customers in Ireland showed that CES could provide residents with more convenient and economical channels for purchasing energy.

Currently, much attention is directed towards exploring sharing models and investigating operational strategies or economic dispatch methods. Few studies have addressed capacity configurations for energy storage devices and the maximization of their economic benefits over their life cycle. Most scholars focus solely on electricity in energy-sharing services.

Hybrid energy storage can cope with future multi-energy coupling and improve the flexibility of energy storage systems, garnering significant interest from researchers [18]. Hydrogen frequently serves a crucial function in hybrid energy storage systems owing to its high energy density, eco-friendliness, and convenient transportability [19]. It is widely regarded as essential for shifting away from the current reliance on fossil fuels and advancing toward a holistic sustainable energy transition. [20]. Reference [21] constructed a distributed robustness-based hybrid energy storage model for electricity and hydrogen in the MMS. This model ensures system economy and can cope with fluctuating renewable energy output. Reference [22] proposed a bi-level optimization model that integrates hydrogen energy with shared energy storage. This approach not only meets the demand of the external hydrogen energy market but also provides microgrid users with greater flexibility in buying and selling energy. Reference [23] proposed hybrid shared energy storage models with different emphases for three different types of regionally integrated energy systems: residential, industrial, and commercial. Although the above literature can enhance the system's economic performance, it lacks a more comprehensive consideration of hydrogen energy circulation. Most studies focus on utilizing the hydrogen generated by shared energy storage either as fuel for power generation or directly selling it to external energy markets, without accounting for the growing internal hydrogen demand within the system.

Addressing the previously identified issues, this paper proposes a bi-level optimization model of configurations and scheduling for the MMS considering shared hybrid electric-hydrogen energy storage service. It can address both the operation optimization for the MMS and the capacity configuration for hybrid energy storage station (HESS). Firstly, the framework structure and operational mode of the proposed service are presented. Subsequently, the simplification and solving process of the complex bi-level optimization model are illustrated. This includes using the KKT conditions and the Big-M method to simplify the model for direct solving by the CPLEX solver. Finally, the economic feasibility and reasonableness of the proposed scheme are verified through a simulation example. The contributions are outlined as follows:

1) Building upon traditional electricity sharing, this study proposes a more advanced shared hybrid electric-hydrogen energy storage service. A bi-level optimization algorithm is employed to address the complex interest interactions between the operator and the MMS, while simultaneously balancing the benefits of both parties.

2) By introducing hydrogen energy flow from HESS to MMS in the model, the approach facilitates more flexible multi-energy transmission within the system while supplying hydrogen to the microgrid at below-market prices.
3) The paper analyzes the operation and profitability of the proposed scheme, providing useful references for industry practitioners.

## 1 System Design

In current energy systems, shared energy storage has become a viable strategy to enhance resource utilization and reduce investment costs [24]. Three prevalent models are widely adopted [25]:

1) Operator-Invested Centralized Shared Energy Storage Station: An independent operator invests in and constructs a large-scale centralized energy storage facility. The primary revenue streams are derived from service fees, energy arbitrage, and capacity leasing. This approach reduces individual investment burdens while ensuring high utilization efficiency.
2) Jointly Invested Shared Energy Storage Station: Multiple energy storage users collaboratively invest in a shared storage facility. By pooling resources, participants mitigate high initial capital expenditures while gaining access to reliable energy storage services. This cooperative model promotes cost-sharing and minimizes idle capacity.
3) User-Leased Energy Storage Equipment: End-users with privately owned energy storage devices lease their idle capacity to others, creating an additional revenue stream. This decentralized model maximizes equipment utilization and facilitates energy circulation across the broader grid.

An increasing number of pilot projects have emerged and achieved significant results. In China's Gansu Province, a 500 MW/1000 MWh project offers capacity leasing at just CNY 250 per kW/year—far lower than the cost of building private facilities. Meanwhile, projects in California have achieved over 80% utilization rates in ancillary services markets, significantly outperforming traditional distributed storage systems.

To avoid conflicts of interest between multiple users and reduce the complexity of implementation, this paper adopts the first service model mentioned above. Furthermore, based on single-energy sharing, a new hybrid energy sharing model is proposed to facilitate more efficient and flexible energy transmission. The corresponding system architecture is illustrated in Fig. 1.

### *1.1 Framework*

As shown in the upper part of Fig. 1, HESS consists of an electricity storage station (ESS) and a hydrogen storage station (HSS), where HSS consists of a P2G device and a tank to store hydrogen. In HESS, both the stored and consumed electrical energy originate from MMS. Excess power generated by the microgrid can be utilized, stored or converted into hydrogen through the dispatch center in HESS. The electricity stored in HESS fills the power gap of MMS. And the hydrogen in it can be supplied to the outside market and to microgrid users who need it.

The structure of CCHP microgrids is shown at the bottom of Fig. 1. Each microgrid is fitted with a range of energy conversion and utilization devices, including gas turbines, heat exchangers, waste heat boilers, gas boilers, electric chillers, absorption chillers, etc. Microgrids are connected to the power grid. However, considering the technical requirements for backward transmission and related policy restrictions, this paper assumes that microgrids cannot sell electricity to the power grid [26]. HESS and microgrids act as independent operating entities, both seeking to maximize their respective benefits through the interactions involving electricity and hydrogen energy.

### *1.2 Operation*

A dispatch center is established within HESS. Users interested in joining the energy storage service need to provide the dispatch center with hourly-resolved annual forecasts of their load demand, renewable generation, and electricity purchase prices. Upon collecting the user-submitted forecast data, the dispatch center performs data cleaning and processing to eliminate outliers and ensure consistency. The processed dataset is then clustered into multiple representative typical days to reduce computational complexity while preserving key variability. Based on these typical days, the dispatch center calculates the optimized capacity of HESS and the operational costs for users. Once both parties reach an agreement, the service agreement is signed, specifying the device capacity, charging and discharging plans, and rules for the payment of service fees, among other details.

ESS and HSS provide energy storage assistance to users in their respective service areas. ESS can absorb some of the excess power from microgrids while delivering power to users in need. In contrast to conventional power stations, the buses of ESS are connected to the microgrid users separately, which allows the transfer of energy at the spatial level through the buses [27]. During a specific period, if the energy demand of all users connected to the ESS bus requires charging, ESS will receive discharging instructions from the dispatch center. Conversely, if the users generate excess electricity, ESS will store excess electricity. HSS produces hydrogen from purchased elec-

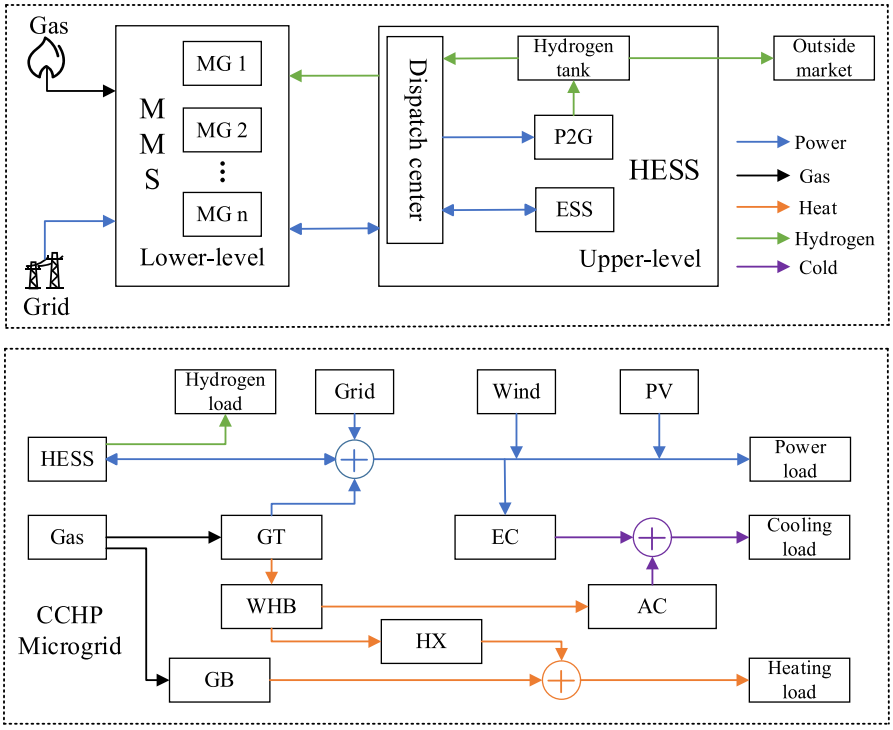


Fig. 1. Structure of the shared hybrid electric-hydrogen energy storage service.

trical energy and sells it to needy users. Hydrogen energy will first be used to meet the demand of microgrid users, and any surplus hydrogen energy will then be transferred to the outside market. This paper considers hydrogen tanker transport for hydrogen energy transmission. Unlike the energy transmission mode of ESS, HSS allows for simultaneous input and output of energy.

The service fee is charged to users by the HESS operator for accessing energy storage capabilities, and it is paid when users interact with ESS or sell power to HSS. Although power exchanges between microgrids do not occur directly through ESS, they are still billed in a manner that simulates flow into and out of ESS. Operators gain revenue in two ways: first, by charging users for their services, and second, by purchasing energy at low prices and selling it at high prices. For the convenience of subsequent calculations, this paper uniformly equates hydrogen energy to electric power.

## 2 Bi-level optimization model building

Bi-level optimization is suitable for addressing system optimization problems that feature distinct primary and secondary models. Typically, the upper part serves as the primary model, while the lower part serves as the secondary one. Both levels have their own objective functions and constraint sets. The optimization procedure initiates at the upper model, where decision variables are determined and subsequently transmitted to the lower model. Upon receipt of this data, the lower model establishes its feasible domain and carries out optimization tasks aimed at achieving the optimal value of its objective function. These outcomes are then relayed back to the upper model. Through iterative processes, the optimal value for the comprehensive model is attained. This optimization method tightly integrates the upper and lower levels of fostering mutual influence and constraint while considering the interests of both parties.

### 2.1 Upper-level HESS model

This model is tasked with optimizing the maximum annual profit of HESS during the planning period. The decision variables consist of two parts. One part is the capacity configurations and maximum power of HESS. The other part is the energy interaction of HESS with the microgrid and the hydrogen energy market.

#### 2.1.1 Objective function of HESS

Based on the decision variables described above, the objective function can be formulated below:

$$\min C = \sum_{m=1}^{M}[T_m(C_{\mathrm{inv},m,\mathrm{ess}} + C_{\mathrm{inv},m,\mathrm{hss}} + C_{\mathrm{ess},m,\mathrm{s}} + C_{\mathrm{hss},m,\mathrm{s}} + C_{\mathrm{trans},m} - C_{\mathrm{serve},m} - C_{\mathrm{ess},m,\mathrm{b}} - C_{\mathrm{hss},m,\mathrm{b}} - C_{\mathrm{hss},m,\mathrm{q}})] \quad (1)$$

where:$M$ is the number of chosen typical days;$T_m$ is the number of days corresponding to the $m-th$ typical day; $C_{\mathrm{inv},m,\mathrm{ess}}$ and $C_{\mathrm{inv},m,\mathrm{hss}}$ are the daily investment costs of ESS and HSS on $m-th$ day, respectively;$C_{\mathrm{ess},m,\mathrm{s}}$ and $C_{\mathrm{hss},m,\mathrm{s}}$ are the purchasing costs of electricity for ESS and HSS on $m-th$ day, respectively;$C_{\mathrm{trans},m}$ is the transporting costs of hydrogen on $m-th$ day;$C_{\mathrm{serve},m}$ is the service revenue from microgrids on $m-th$ day;$C_{\mathrm{ess},m,\mathrm{b}}$ is the revenue generated by selling electricity on $m-th$ day;$C_{\mathrm{hss},m,\mathrm{b}}$ and $C_{\mathrm{hss},m,\mathrm{q}}$ are the revenue generated by selling hydrogen from HSS to microgrids and to the outside market on $m-th$ day, respectively.

1) The daily investment cost of ESS can be described as:

$$C_{\mathrm{inv},m,\mathrm{ess}}=\frac{\alpha_{\mathrm{ess}}P_{\mathrm{ess}}^{\max}+\beta_{\mathrm{ess}}E_{\mathrm{ess}}^{\max}}{T_{\mathrm{ess}}}+Y_{\mathrm{ess}} \tag{2}$$

where:$\alpha_{\mathrm{ess}}$ and $\beta_{\mathrm{ess}}$ are the per-unit power cost and capacity cost of ESS, respectively;$P_{\mathrm{ess}}^{\max}$ and $E_{\mathrm{ess}}^{\max}$ are the maximum power and maximum capacity of ESS, respectively;$T_{\mathrm{ess}}$ is the serve days of ESS;$Y_{\mathrm{ess}}$ is the maintenance cost of ESS per day.

2) The daily investment cost of HSS can be described as:

$$C_{\mathrm{inv},m,\mathrm{hss}}=\frac{\alpha_{\mathrm{p2g}}P_{\mathrm{p2g}}^{\max}}{T_{\mathrm{p2g}}}+\frac{\beta_{\mathrm{tank}}E_{\mathrm{tank}}^{\max}}{T_{\mathrm{tank}}}+Y_{\mathrm{p2g}}+Y_{\mathrm{tank}} \tag{3}$$

where:$\alpha_{\mathrm{p2g}}$ is the per-unit power cost of the P2G device;$\beta_{\mathrm{tank}}$ is the per-unit capacity cost of the hydrogen storage tank;$P_{\mathrm{p2g}}^{\max}$ and $E_{\mathrm{tank}}^{\max}$ are the maximum power and maximum capacity of the P2G device and hydrogen storage tank, respectively;$T_{\mathrm{p2g}}$ and $T_{\mathrm{tank}}$ are the serve days of the P2G device and hydrogen storage tank, respectively;$Y_{\mathrm{p2g}}$ and $Y_{\mathrm{tank}}$ are the maintenance costs of the P2G device and hydrogen storage tank per day, respectively.

3) The purchasing cost of electricity for ESS can be described as:

$$C_{\mathrm{ess},m,\mathrm{s}}=\sum_{r=1}^{N}\sum_{t=1}^{N_T}\Delta t\cdot\varphi_{\mathrm{d}}^{\mathrm{buy}}(t)\cdot P_{\mathrm{ess},\mathrm{s},m,r}(t) \tag{4}$$

where:$N$ is the number of microgrids;$N_T$ is the number of scheduling periods;$\Delta t$ is the time interval.$\varphi_{\mathrm{d}}^{\mathrm{buy}}(t)$ is the selling price of electricity to ESS by microgrids at time $t$;$P_{\mathrm{ess},\mathrm{s},m,r}(t)$ is the electricity sold to ESS by microgrid $r$ at time $t$ on $m-th$ day.

4) The purchasing cost of electricity for HSS can be described as:

$$C_{\mathrm{hss},m,\mathrm{s}}=\sum_{r=1}^{N}\sum_{t=1}^{N_T}\Delta t\cdot\varphi_{\mathrm{h}}^{\mathrm{buy}}(t)\cdot P_{\mathrm{hss},\mathrm{s},m,r}(t) \tag{5}$$

where:$\varphi_{\mathrm{h}}^{\mathrm{buy}}(t)$ is the selling price of electricity to HSS by microgrids at time $t$;$P_{\mathrm{hss},\mathrm{s},m,r}(t)$ is the electricity sold to HSS by microgrid $r$ at time $t$ on $m-th$ day.

5) Transporting costs of hydrogen can be described as [28]:

$$C_{\mathrm{trans},m}=\frac{P_{\mathrm{hss},\mathrm{b},m,r}(t)\cdot(0.334S_r+2.771)}{\eta_{\mathrm{h_2}}^{\mathrm{trans}}} \tag{6}$$

where:$P_{\mathrm{hss},\mathrm{b},m,r}(t)$ is the hydrogen purchased from HSS by microgrid $r$ at time $t$ on $m-th$ day;$S_r$ is the distance of microgrid $r$ from HSS, and the unit is kilometers;$\eta_{\mathrm{h_2}}^{\mathrm{trans}}$ is the factor used to convert 1 kW of hydrogen to its mass equivalent.

6) The service revenue can be described as:

$$C_{\mathrm{serve},m}=\sum_{r=1}^{N}\sum_{t=1}^{N_T}\{\varphi(t)\cdot\Delta t[P_{\mathrm{hss},\mathrm{s},m,r}(t)+P_{\mathrm{ess},\mathrm{s},m,r}(t)+P_{\mathrm{ess},\mathrm{b},m,r}(t)]\} \tag{7}$$

where:$\varphi(t)$ is the service fee for each unit of electricity traded;$P_{\mathrm{ess},\mathrm{b},m,r}(t)$ is the electricity purchased from ESS by microgrid $r$ at time $t$ on $m-th$ day.

7) The revenue generated by selling electricity can be described as:

$$C_{\mathrm{ess},m,\mathrm{b}}=\sum_{r=1}^{N}\sum_{t=1}^{N_T}\Delta t\cdot\varphi_{\mathrm{d}}^{\mathrm{sell}}(t)\cdot P_{\mathrm{ess},\mathrm{b},m,r}(t) \tag{8}$$

where:$\varphi_{\mathrm{d}}^{\mathrm{sell}}(t)$ is the purchasing price of electricity from ESS at time $t$.

8) The revenue generated by selling hydrogen from HSS to microgrids can be described as:

$$C_{\mathrm{hss},m,\mathrm{b}}=\sum_{r=1}^{N}\sum_{t=1}^{N_T}\Delta t\cdot\varphi_{\mathrm{h}}^{\mathrm{sell}}(t)\cdot P_{\mathrm{hss},\mathrm{b},m,r}(t) \tag{9}$$

where:$\varphi_{\mathrm{h}}^{\mathrm{sell}}(t)$ is the purchasing price of hydrogen from HSS by microgrids at time $t$.

9) The revenue generated by selling hydrogen from HSS to the outside market can be described as:

$$C_{\mathrm{hss},m,\mathrm{q}}=\Delta t\cdot\varphi_{\mathrm{q}}^{\mathrm{sell}}(t)\cdot P_{\mathrm{hss},\mathrm{q},m}(t) \tag{10}$$

where:$\varphi_{\mathrm{q}}^{\mathrm{sell}}(t)$ is the purchasing price of hydrogen from HSS by the outside market at time $t$;$P_{\mathrm{hss},\mathrm{q},m}(t)$ is the hydrogen purchased from HSS by the outside market at time $t$ on $m-th$ day.

*2.1.2 Effects of equipment degradation*

In this section, a linear degradation model for HESS is introduced to enable a more comprehensive evaluation of the system's economic performance. The model primarily considers the linear degradation of ESS capacity over time as well as the linear efficiency decline of P2G equipment. At the same time, it is assumed that no parameter degradation occurs during a typical operational day. Parameter adjustments, incorporating linear decay, are implemented only upon completion of each typical day.

$$\begin{cases} E_{\mathrm{ess},m}^{\max} = (1-k_{\mathrm{ess},m})E_{\mathrm{ess}}^{\max} \\ \eta_{\mathrm{hss},m}^{\mathrm{abs}} = (1-k_{\mathrm{hss},m})\eta_{\mathrm{hss}}^{\mathrm{abs}} \end{cases} \tag{11}$$

where:$E_{\mathrm{ess},m}^{\max}$ and $\eta_{\mathrm{hss},m}^{\mathrm{abs}}$ are the ESS capacity and P2G efficiency corresponding to the $m-th$ typical day, respectively;$k_{\mathrm{ess},m}$ and $k_{\mathrm{hss},m}$ are the ESS capacity and P2G efficiency degradation coefficients corresponding to the $m-th$ typical day, respectively; $\eta_{\mathrm{hss}}^{\mathrm{abs}}$ is the power-to-hydrogen conversion efficiency of P2G.

*2.1.3 Constraints of HESS*

1) The ratio of capacity to rated power [22] can be defined as:

$$\begin{cases} E_{\mathrm{ess}}^{\max} = \delta_{\mathrm{ess}}P_{\mathrm{ess}}^{\max} \\ E_{\tan k}^{\max} = \delta_{\mathrm{hss}}P_{\mathrm{p2g}}^{\max} \end{cases} \tag{12}$$

where:$\delta_{\mathrm{ess}}$ and $\delta_{\mathrm{hss}}$ are the ratio of ESS and HSS, respectively.

2) Charging and discharging constraints of ESS on the $m-th$ typical day can be described as:

$$\begin{gathered} E_{\mathrm{ess},m}(t) = \Delta t\cdot[\eta_{\mathrm{ess}}^{\mathrm{abs}}P_{\mathrm{ess,abs},m}(t) - \tfrac{1}{\eta_{\mathrm{ess}}^{\mathrm{rel}}}P_{\mathrm{ess,rel},m}(t)] + E_{\mathrm{ess},m}(t-1) \\ 10\%E_{\mathrm{ess},m}^{\max} \le E_{\mathrm{ess}}(t) \le 90\%E_{\mathrm{ess},m}^{\max} \\ 0 \le P_{\mathrm{ess,abs},m}(t) \le P_{\mathrm{ess},m}^{\max}U_{\mathrm{abs}}(t) \\ 0 \le P_{\mathrm{ess,rel},m}(t) \le P_{\mathrm{ess},m}^{\max}U_{\mathrm{rel}}\ (t) \\ U_{\mathrm{abs}}\ (t) + U_{\mathrm{rel}}\ (t) \le 1 \\ U_{\mathrm{abs}}\ (t) \in \{0,1\}, U_{\mathrm{rel}}\ (t) \in \{0,1\} \end{gathered} \tag{13}$$

where:$E_{\mathrm{ess},m}(t)$ is the electricity stock in ESS at time $t$;$\eta_{\mathrm{ess}}^{\mathrm{abs}}$ and $\eta_{\mathrm{ess}}^{\mathrm{rel}}$ are efficiencies of charging and discharging for ESS;$P_{\mathrm{ess,abs},m}(t)$ and $P_{\mathrm{ess,rel},m}(t)$ are the power of charging and discharging for ESS at time $t$, respectively;$U_{\mathrm{abs}}(t)$ and $U_{\mathrm{rel}}(t)$ are states of charging and discharging, which are both 0–1 variables.

3) Charging and discharging constraints of HSS on the $m-th$ typical day can be described as:

$$\begin{gathered} E_{\mathrm{tank},m}(t) = \Delta t\cdot[\eta_{\mathrm{hss},m}^{\mathrm{abs}}P_{\mathrm{hss,abs},m}(t) - \tfrac{P_{\mathrm{hss,rel},m}(t)}{\eta_{\mathrm{hss}}^{\mathrm{rel}}}] + E_{\tan k,m}(t-1) \\ 10\%E_{\tan k}^{\max} \le E_{\tan k,m}(t) \le 90\%E_{\tan k}^{\max} \\ 0 \le P_{\mathrm{hss,abs},m}(t) \le P_{\mathrm{p2g}}^{\max} \\ 0 \le P_{\mathrm{hss,rel},m}(t) \le P_{\mathrm{trans}}^{\max} \end{gathered} \tag{14}$$

where:$E_{\mathrm{tank},m}(t)$ is the hydrogen stock in HSS at time $t$;$\eta_{\mathrm{hss}}^{\mathrm{rel}}$ is the hydrogen discharging efficiency;$P_{\mathrm{hss,abs},m}(t)$ and $P_{\mathrm{hss,rel},m}(t)$ are the charging and discharging power of HSS at time $t$, respectively;$P_{\mathrm{trans}}^{\max}$ is the maximum hydrogen energy delivery power.

4) Constraints between HSS and the outside market can be described as:

$$0 \le P_{\mathrm{hss,q},m}(t) \le P_{\mathrm{hload},m}(t) \tag{15}$$

where:$P_{\mathrm{hload},m}(t)$ is the hydrogen load of the outside market on $m-th$ day.

*2.2 Lower-level MMS model*

This model is tasked with optimizing the minimum annual operating cost of the MMS during the planning period. Decision variables include outputs of devices within microgrids, power interactions between the main power grid and microgrids and their corresponding states, as well as power interactions between HESS and microgrids and their respective states.

*2.2.1 Objective function of the MMS*

The optimization seeks to minimize the annual operating cost of the MMS, which can be described as:

$$\begin{aligned} \min C = \sum_{m=1}^{M}[T_m(&C_{\mathrm{grid},m} + C_{\mathrm{fuel},m} + C_{\mathrm{ess},m,\mathrm{b}} + C_{\mathrm{serve},m} \\ &+ C_{\mathrm{hss},m,\mathrm{b}} - C_{\mathrm{ess},m,\mathrm{s}} - C_{\mathrm{hss},m,\mathrm{s}})] \end{aligned} \tag{16}$$

where:$C_{\mathrm{grid},m}$ is the purchasing cost from the power grid by microgrids on $m-th$ day;$C_{\mathrm{fuel},m}$ is the cost of gas on $m-th$ day; .

1) The purchasing cost from the power grid can be described as:

$$C_{\mathrm{grid},m} = \sum_{r=1}^{N}\sum_{t=1}^{N_T}\Delta t\cdot\varphi_{\mathrm{grid}}(t)\cdot P_{\mathrm{grid},m,r}(t) \tag{17}$$

where:$\varphi_{\mathrm{grid}}(t)$ is the grid tariff at time $t$;$P_{\mathrm{grid},m,r}(t)$ is the electricity purchased from the power grid by microgrid $r$ at time $t$ on $m-th$ day.

2) The cost of gas can be described as:

$$C_{\text{fuel},m} = \varphi_{\text{gas}} \sum_{r=1}^{N} \sum_{t=1}^{N_T} \Delta t \cdot [\frac{P_{\text{GT},m,r}(t)}{\eta_{\text{GT}} L_{\text{NG}}} + \frac{Q_{\text{GB},m,r}(t)}{\eta_{\text{GB}} L_{\text{NG}}}] \tag{18}$$

where:$\varphi_{\text{gas}}$ is the per-unit price of gas;$P_{\text{GT},m,r}(t)$ is the power output of the gas turbine in microgrid $r$ at time $t$ on $m-th$ day;$\eta_{\text{GT}}$ and $\eta_{\text{GB}}$ are the efficiencies of the gas turbine and gas boiler, respectively;$L_{\text{NG}}$ is the low heating value of gas, which is 9.7 kW·h/m$^3$;$Q_{\text{GB},m,r}(t)$ is the thermal output of the gas boiler in microgrid $r$ at time $t$ on $m-th$ day.

*2.2.2 Constraints of the MMS*

Some equation constraints that need to be met for the optimal operation of the MMS are listed below:

1) Electrical power balance can be described as:

$$\begin{aligned} &P_{\text{grid},m,r}(t) + P_{\text{GT},m,r}(t) + P_{\text{ess,b},m,r}(t) + P_{\text{WT},m,r}(t) + P_{\text{PV},m,r}(t) \\ &\quad = P_{\text{ess,s},m,r}(t) + P_{\text{hss,s},m,r}(t) + P_{\text{load},m,r}(t) + P_{\text{EC},m,r}(t) \end{aligned} \tag{19}$$

where:$P_{\text{PV},m,r}(t)$ and $P_{\text{WT},m,r}(t)$ are the photovoltaic power and the wind power of microgrid $r$ at time $t$ on $m-th$ day, respectively; $P_{\text{EC},m,r}(t)$ is the electricity consumed by the electric chiller in microgrid $r$ at time $t$ on $m-th$ day;$P_{\text{load},m,r}(t)$ is the electrical load in microgrid $r$ at time $t$ on $m-th$ day.

2) Cooling power balance can be described as:

$$P_{\text{EC},m,r}(t)\eta_{\text{EC}} + Q_{\text{AC},m,r}(t) = P_{\text{cool},m,r}(t) \tag{20}$$

where:$\eta_{\text{EC}}$ is the performance coefficient of the electric chiller;$Q_{\text{AC},m,r}(t)$ is the cooling power output of the absorption chiller in microgrid $r$ at time $t$ on $m-th$ day;$P_{\text{cool},m,r}(t)$ is the cooling load of microgrid $r$ on $m-th$ day.

3) Heating power balance can be described as:

$$Q_{\text{GB},m,r}(t) + P_{\text{HX},m,r}(t) = P_{\text{heat},m,r}(t) \tag{21}$$

where:$P_{\text{HX},m,r}(t)$ is the output of heating power in microgrid $r$ at time $t$ on $m-th$ day;$P_{\text{heat},m,r}(t)$ is the heating load of microgrid $r$ at time $t$ on $m-th$ day.

4) Waste heat balance can be described as:

$$\frac{P_{\text{HX},m,r}(t)}{\eta_{\text{HX}}} + \frac{Q_{\text{AC},m,r}(t)}{\eta_{\text{AC}}} = \gamma_{\text{GT}}\eta_{\text{WH}}P_{\text{GT},m,r}(t) \tag{22}$$

where:$\eta_{\text{HX}}$ and $\eta_{\text{WH}}$ are the efficiency of the heat exchanger and waste heat boiler;$\eta_{\text{AC}}$ is the performance coefficient of the absorption chiller;$\gamma_{\text{GT}}$ is the power-to-heat ratio of the gas turbine.

5) Charging and discharging the balance of ESS can be described as:

$$\sum_{i=1}^{N}[P_{\text{ess,s},m,r}(t) - P_{\text{ess,b},m,r}(t)] = P_{\text{ess,abs},m}(t) - P_{\text{ess,rel},m}(t) \tag{23}$$

6) Charging balance of HSS can be described as:

$$\sum_{i=1}^{N} P_{\text{hss,s},m,r}(t) = P_{\text{hss,abs},m}(t) \tag{24}$$

7) Discharging balance of HSS can be described as:

$$P_{\text{hss,q},m}(t) + \sum_{i=1}^{N} P_{\text{hss,b},m,r}(t) = P_{\text{hss,rel},m}(t) \tag{25}$$

8) Hydrogen load balance can be described as:

$$P_{\text{hss,b},m,r}(t) = P_{\text{hload},m,r}(t) \tag{26}$$

where:$P_{\text{hload},m,r}(t)$ is the hydrogen load of microgrid $r$ at time $t$ on $m-th$ day.

It also needs to satisfy the inequality constraints as follows:

1) Constraints of output can be described as:

$$\begin{cases} P_{\text{GT}}^{\min} \le P_{\text{GT},m,r}(t) \le P_{\text{GT}}^{\max} \\ Q_{\text{AC}}^{\min} \le Q_{\text{AC},m,r}(t) \le Q_{\text{AC}}^{\max} \\ P_{\text{EC}}^{\min} \le P_{\text{EC},m,r}(t) \le P_{\text{EC}}^{\max} \\ Q_{\text{GB}}^{\min} \le Q_{\text{GB},m,r}(t) \le Q_{\text{GB}}^{\max} \\ P_{\text{HX}}^{\min} \le P_{\text{HX},m,r}(t) \le P_{\text{HX}}^{\max} \end{cases} \tag{27}$$

where: the above are maximum and minimum values for each device, respectively.

2) Constraints of energy interaction with the power grid can be described as:

$$0 \le P_{\text{grid},m,r}(t) \le P_{\text{grid,mg}}^{\max} \tag{28}$$

where:$P_{\text{grid,mg}}^{\max}$ is the maximum electric power that microgrids can purchase from the power grid.

3) Constraints of energy interaction with ESS can be described as:

$$\begin{cases} 0 \le P_{\text{ess,b},m,r}(t) \le P_{\text{ess,mg}}^{\max} U_{\text{b},m,r}(t) \\ 0 \le P_{\text{ess,s},m,r}(t) \le P_{\text{ess,mg}}^{\max} U_{\text{s},m,r}(t) \\ U_{\text{b},m,r}(t) + U_{\text{s},m,r}(t) \le 1 \end{cases} \tag{29}$$

where:$U_{\text{b},m,r}(t)$ and $U_{\text{s},m,r}(t)$ are the state bits of microgrid on $m-th$ day, representing purchase and sale, respec-

tively;$P^{\max}_{\mathrm{ess,mg}}$ is the maximum power that can be exchanged between ESS and microgrids.

4) Constraints of energy interaction with HSS can be described as:

$$\begin{cases} 0 \le P_{\mathrm{hss,s},m,r}(t) \le P^{\max}_{\mathrm{hss,mg}} \\ 0 \le P_{\mathrm{hss,b},m,r}(t) \le P^{\max}_{\mathrm{hss,hmg}} \end{cases} \tag{30}$$

where:$P^{\max}_{\mathrm{hss,mg}}$ is the maximum power sold to HSS;$P^{\max}_{\mathrm{hss,hmg}}$ is the maximum power purchased from HSS.

## 3 Model solving process based on bi-level optimization

As illustrated in Fig. 2, the solution process for the proposed shared hybrid electric-hydrogen energy storage service consists of three main stages: data input, model construction, and bi-level optimization model simplification.

The input data includes two key components: the annual forecasted load and output of renewable energy units, and the energy price information for interactions among stakeholders. The annual forecast data undergoes preprocessing—such as feature extraction and data cleaning—before being processed using the K-means clustering method to generate representative typical daily datasets.

The bi-level optimization model, detailed in the previous chapter, comprises an upper-level model with integer and continuous variables under nonlinear constraints, and a lower-level model formulated as a mixed-integer linear program. Both levels aim to maximize their respective objectives, resulting in a complex interdependence.

Due to the strong coupling between the two levels, direct computation is intractable. To address this, the Lagrangian function of the lower-level model is first constructed. The lower-level model is then transformed into upper-level constraints using the KKT complementary slackness conditions, as shown in Appendix A (Equations A2–A40). Next, nonlinearities in the converted model are linearized via the Big-M method (Appendix A, Equations A41–A43), yielding a single-layer MILP formulation. Finally, the simplified MILP model is solved using the commercial solver CPLEX in MATLAB, outputting the optimal hybrid energy storage configuration and microgrid operation results.

## 4 Case study

### 4.1 Parameter setting

Three disconnected CCHP microgrids, namely MG 1, MG 2, and MG 3, are selected to constitute an MMS. Each microgrid is directly connected to HESS, with distances of 50 km, 80 km, and 120 km, respectively. MG1 is a power-abundant microgrid characterized by high wind and photovoltaic output, while MG2 represents a balanced energy supply–demand microgrid without wind turbines. In contrast, MG3 is an energy-deficient microgrid with significant load demand. Considering the significant impact of seasonal variations on microgrids, the K-means clustering method is adopted to cluster the forecast data of spring, summer, autumn, and winter into four typical days to simulate the annual operation of MMS. Each season consists of 91 days, and each day is 24 h long. The clustered data of microgrids are illustrated in Fig. B1 of Appendix B. The hydrogen load in the outside market after clustering is depicted in Fig. B2 of Appendix B. The gas price is taken as the industrial gas price, 3.42CNY/m$^3$. The economic parameters of various devices in HESS can be found in Table 1. Table 2 illustrates the pricing for electricity and hydrogen interactions among the power grid, microgrids, HESS, and the outside market. The unit power cost for the service is 0.05CNY/kWh. Equipment-related parameters are provided in Appendix C, Table C1.

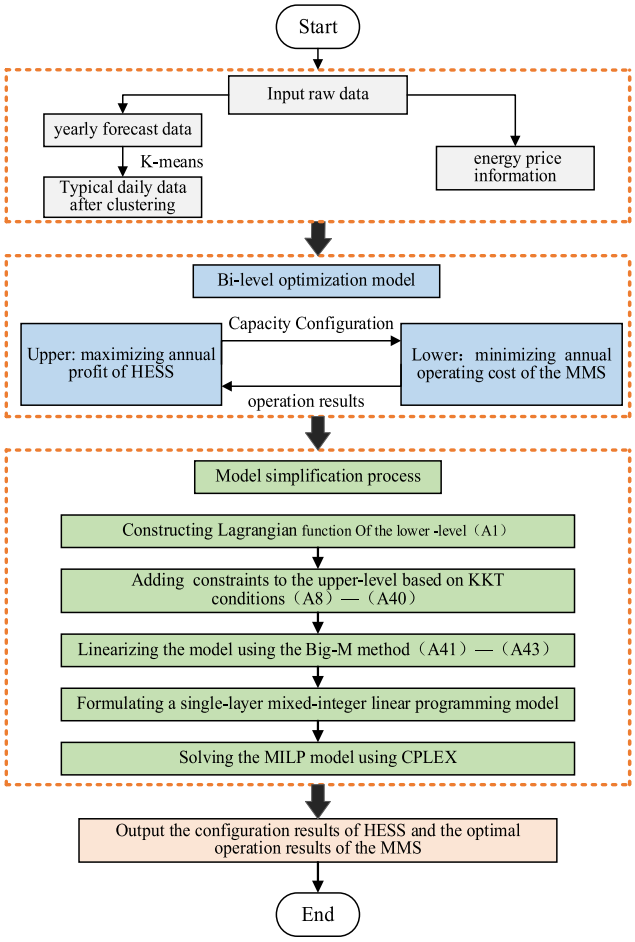


Fig. 2. Flowchart for solving the bi-level model of shared hybrid electric-hydrogen energy storage service.

To validate the advantages of the proposed shared HESS service, a comparative analysis of three scenarios is conducted:

1) The MMS without additional energy storage equipment.
2) The MMS participates in the shared ESS service.
3) The MMS participates in the shared HESS service.

### 4.2 Optimization results

Under the three cases, the annual operating cost of the MMS, the annual profit of the operator, and the renewable energy absorption rate are shown in Table 3. In Case 1, there is no additional energy storage equipment incorporated into the MMS. Excess energy is wasted, and power shortages are compensated by purchasing from the power grid. Its annual operating cost is 37,759,034 CNY, with a renewable energy absorption rate of only 69.78%, leading to significant wastage.

After participating in shared electric energy storage service, the power purchase of the MMS is more flexible and versatile. Excess electricity can also be sold to ESS, generating additional revenue and avoiding energy waste. The annual operating cost of the MMS decreased to 31,355,549 CNY, a decrease of 16.96% from Case 1. Renewable energy absorption rate increased to 100%. In addition, the operator receives a considerable amount of profit, amounting to 3,557,835 CNY annually.

In Case 3, hydrogen trading is incorporated into the shared energy storage service, providing users with hydrogen energy at prices substantially below market rates, while further enhancing the flexibility of microgrid users in both purchasing and selling electricity. The cost of the MMS is 30,152,336 CNY, a decrease of 7,606,698 compared to Case 1, a decrease of approximately 20.15%. Considering the hydrogen demand, the operator's energy sales channels are expanded, with a consequent increase in profit. In this case, the operator can earn 5,717,427 CNY in annual profit. This is a rise of 2,159,592 CNY, nearly 60.71% from Case 2.

The following discusses the advantages of Case 3 compared with Case 2, focusing on the capacity configuration and payback periods. The outcomes of the optimized capacity are presented in Table 4. Due to the consideration of hydrogen demand, the system's electrical energy allocation becomes more flexible. The capacity of ESS decreased by 2,991.69 kWh, representing a reduction of approximately 55.35%, which significantly lowered its cost. However, to meet user demand, a P2G device with a power output of 1,385.85 kW and a hydrogen tank with a capacity of 5,543.40 kWh were added. Although the total equipment investment cost of Case 3 is less advantageous compared to Case 2, by analyzing Tables 1 and 3, it can be concluded that the operator can expect to shorten the payback period due to higher benefits and the longer lifespan of the equipment.

Table 5 demonstrates the payback periods for each device as well as the operator, thus providing a clearer perspective on the economic benefits of the two cases. For both cases, the payback periods for the energy storage equipment are less than their respective lifetimes. It is theoretically feasible for operators to invest in shared energy storage. In Case 2, ESS can achieve payback in 3.59 years by selling electricity and charging a service fee. In Case 3, the addition of hydrogen trading further enhances the benefits. The payback periods for ESS, P2G device, and hydrogen storage tank are 1.64 years, 4.74 years, and 7.20 years, respectively. Operators can recover all equipment construction and maintenance costs in 3.02 years, which is a reduction of 0.57 years. It should be noted that the profits for the P2G device and hydrogen storage tank are calculated by distributing the total HSS revenue according to their investment proportion.

To summarize, the introduction of shared energy storage services can cut down user expenses, achieve a 100% renewable energy absorption rate, and provide considerable benefits to operators. The model introduced in this paper, integrating hydrogen energy with shared energy storage, demonstrates more incredible economic benefits for both users and operators when contrasted with conventional shared electric energy storage service.

### 4.3 Energy interaction

#### 4.3.1 Energy interaction in Case 2

Figs. 3 and 4 illustrate the optimized charging and discharging behavior of ESS and the energy exchange dynamics on the microgrid side in Case 2, respectively. From Fig. 3, it can be observed that during several time periods, such as 14:00–16:00 and 20:00–24:00, the stock change is zero. Power is exchanged solely through the ESS bus, enabling the spatial transfer of energy. For the rest of the time, ESS is in a state of charging or discharging, maintaining the balance of the entire system by exchanging energy with the microgrid. From 00:00 to 08:00, the first accumulation of electricity occurred. Combined with Fig. 4, MG 1

Table 1
Economic parameters of HESS.

| Equipment | Capacity cost CNY/kWh | Power cost CNY/kW | Maintenance cost CNY/kW | Serve years |
|---|---|---|---|---|
| Battery | 1897[29] | 1000[29] | 72[29] | 8[29] |
| P2G | / | 6900[30] | 138[30] | 15[30] |
| Hydrogen tank | 104[30] | / | 2[30] | 25[30] |

Table 2
Energy interactive price list.

| | Time slot | Grid electricity purchase tariff CNY/kW | from ESS CNY/kW | electricity sold to ESS CNY/kW | electricity sold to HSS CNY/kW | Hydrogen sold to microgrids CNY/kW | Hydrogen sold outside CNY/kW | Market price of hydrogen CNY/kW |
|---|---|---|---|---|---|---|---|---|
| Peak | 08:00–12:00<br>17:00–21:00 | 1.36 | 1.15 | 0.95 | 1.06 | 1.13 | 1.39 | 1.51 |
| Shoulder | 12:00–17:00<br>21:00–24:00 | 0.82 | 0.75 | 0.55 | 0.66 | | | |
| Valley | 00:00–08:00 | 0.37 | 0.40 | 0.20 | 0.31 | | | |

Table 3
Comparison of costs, benefits and renewable energy absorption rate under three cases.

| | Annual operating cost of the MMS /$10^4$ CNY | Annual profit of the operator /$10^4$ CNY | Renewable energy absorption |
|---|---|---|---|
| Case1 | 3775.90 | 0 | 69.78% |
| Case2 | 3135.55 | 355.78 | 100% |
| Case3 | 3015.23 | 571.74 | 100% |

Table 4
Outcomes of the optimized capacity configuration in Case 2 and Case 3.

| | Equipment | Power/kW | Capacity /kWh | Cost/$10^4$ CNY |
|---|---|---|---|---|
| Case2 | ESS | 2027.65 | 5405.32 | 1228.15 |
| Case3 | ESS | 905.40 | 2413.63 | 1562.29 |
| | HSS | 1385.85 | 5543.40 | |

imported a significant amount of wind power into ESS during that period. Meanwhile, the two energy-deficient microgrids did not consume too much ESS stock but chose to purchase power from gas companies and the power grid to satisfy their load. After 8:00, the grid electricity prices rise rapidly. Microgrids stop purchasing power from the power grid and instead depend on the cheaper ESS supply. The ESS stock falls rapidly. The second phase of power accumulation occurs between 10:00 and 14:00, driven by a surge in photovoltaic (PV) generation. However, renewable energy generation exhibits inherent intermittency, with PV systems being particularly pronounced in this regard. As solar irradiance diminishes, PV output gradually declines to zero. Consequently, the MMS resumes drawing energy from ESS to maintain load demand.

#### 4.3.2 Energy interaction in Case 3

Fig. 5 illustrates the optimization of charging and discharging for HESS in Case 3. According to Fig. 5(b), HSS discharges are mainly concentrated between 07:00 and 20:00, so hydrogen loads are concentrated during daytime hours. The selling price of electricity for microgrids is highest during 08:00–12:00 and 17:00–21:00 due to the time-of-use tariff. HSS needs to meet its electricity demand while avoiding purchasing at these peak periods. Therefore, the energy charging of HSS is primarily concentrated from 00:00 to 08:00 and from 12:00 to 16:00.

As shown in Fig. 5(a), from 00:00 to 08:00, the energy purchase decisions of ESS and HSS are similar, with both choosing to charge during the low-price period. However, the total charging power of the two stations already exceeds the power supply available from microgrids. Combined with the data shown in Fig. 6, MG 2 and MG 3 both sacrificed some of their own interests during that period to purchase electricity from the grid to maintain the economic efficiency of the entire system.

### 4.4 Sensitivity analysis

Using the renewable energy input data in Section 4.1 as the baseline (with a renewable energy penetration rate of 1), Fig. 7 illustrates the impact of varying penetration rates on the shared hybrid electric-hydrogen energy storage system. In this experiment, the actual renewable energy penetration rate is 58.12%. As shown in the figure, when the penetration rate decreases, the capacity configuration

Table 5
Payback periods for each device and operator in Case 2 and Case 3.

| | Serve years | Payback years in Case2 | Payback years in Case3 |
|---|---|---|---|
| Battery | 8 | 3.59 | 1.64 |
| P2G | 15 | / | 4.74 |
| Hydrogen tank | 25 | / | 7.20 |
| operator | / | 3.59 | 3.02 |

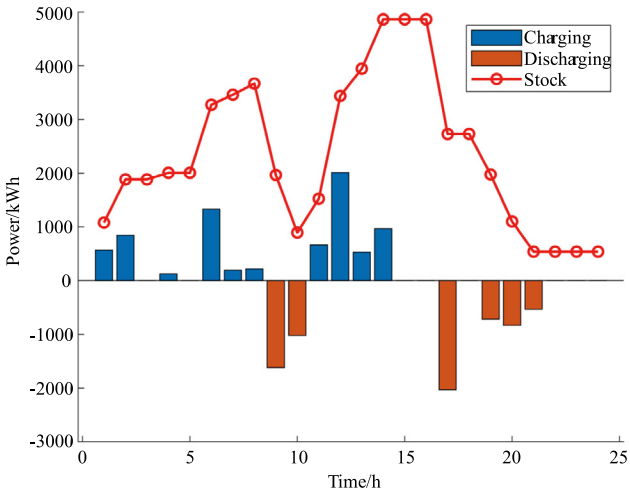


Fig. 3. Optimization of the charging and discharging energy for ESS on a typical spring day in Case 2.

declines accordingly, leading to economic losses for both operator and microgrids.

In the initial stage of increasing penetration rates, microgrids can profit by selling more energy to the stations, while operators can reap greater benefits by deploying slightly larger storage systems. However, if the penetration rate continues to rise beyond a certain threshold, the energy input from the microgrid will far exceed the overall system's load demand. Operators must significantly expand energy storage capacity to accommodate the energy, which will lead to a sharp increase in the initial construction costs of the equipment. This not only reduces the operators' annual revenue but also extends the investment payback period.

### *4.5 Adaptive analysis based on Monte Carlo simulation*

Due to the randomness of wind turbines, PV systems, and loads, the operation of microgrids incorporating shared hybrid electric-hydrogen energy storage is significantly affected. To address this, the Monte Carlo method was employed to randomly generate 1,000 scenarios by combining the renewable energy output characteristics and load profiles of various users. These scenarios cover extreme cases such as peak loads, full output from wind turbines or PV systems, and extremely low generation. By simulating the operation under these scenarios, the optimal operational strategies for each scenario, as well as the economic benefits for users and operators, can be obtained.

Fig. 8 presents a comparison of economic benefits between Case 3 and Case 2 across the 1000 generated scenarios. Positive values indicate that Case 3 has better economic benefits than Case 2. The figure clearly shows that the proposed shared hybrid electric-hydrogen energy storage service is superior to Case 2 in 94.3% of scenarios, achieving a win–win situation for microgrids and opera-

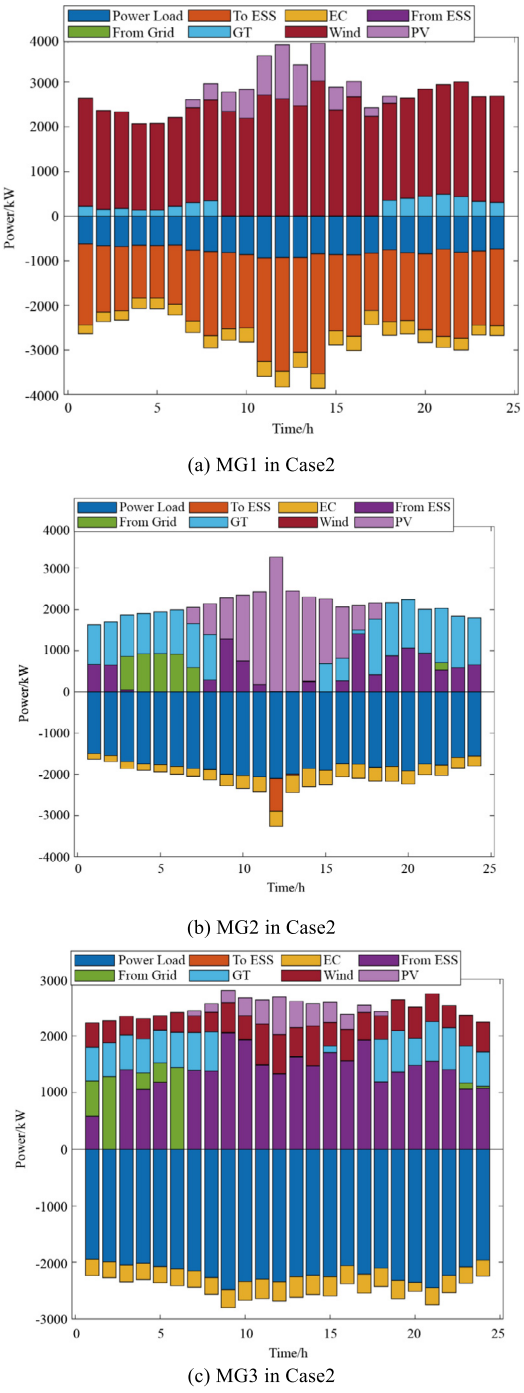


(a) MG1 in Case2

(b) MG2 in Case2

(c) MG3 in Case2

Fig. 4. Optimization of the energy interaction for microgrids on a typical spring day in Case 2.

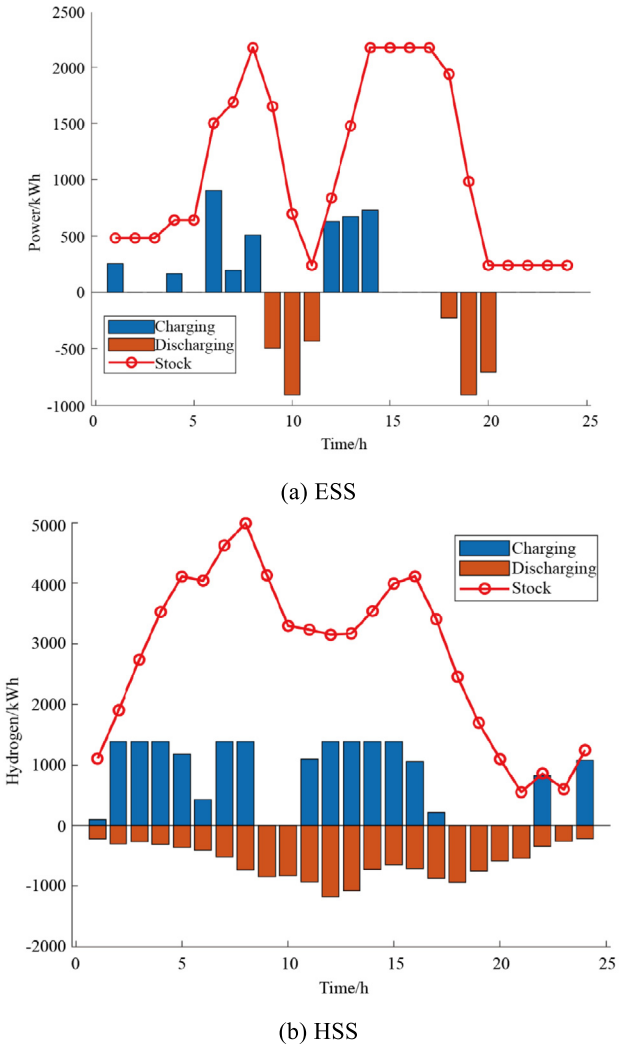


(a) ESS

(b) HSS

Fig. 5. Optimization of the charging and discharging energy for HESS on a typical spring day in Case 3.

tors. In only 0.6% of cases, the proposed scheme is completely inferior to the traditional electricity-sharing model. These results indicate that even when considering uncertainty factors, the proposed scheme remains significantly superior to the traditional model. Monte Carlo simulations comprehensively assess the impact of various uncertainty factors on the model's economic performance, thereby providing robust validation of its reliability. It should be noted that the determination of the benefit boundary is based on the calculation results of the maximum benefit difference between Case 3 and Case 2.

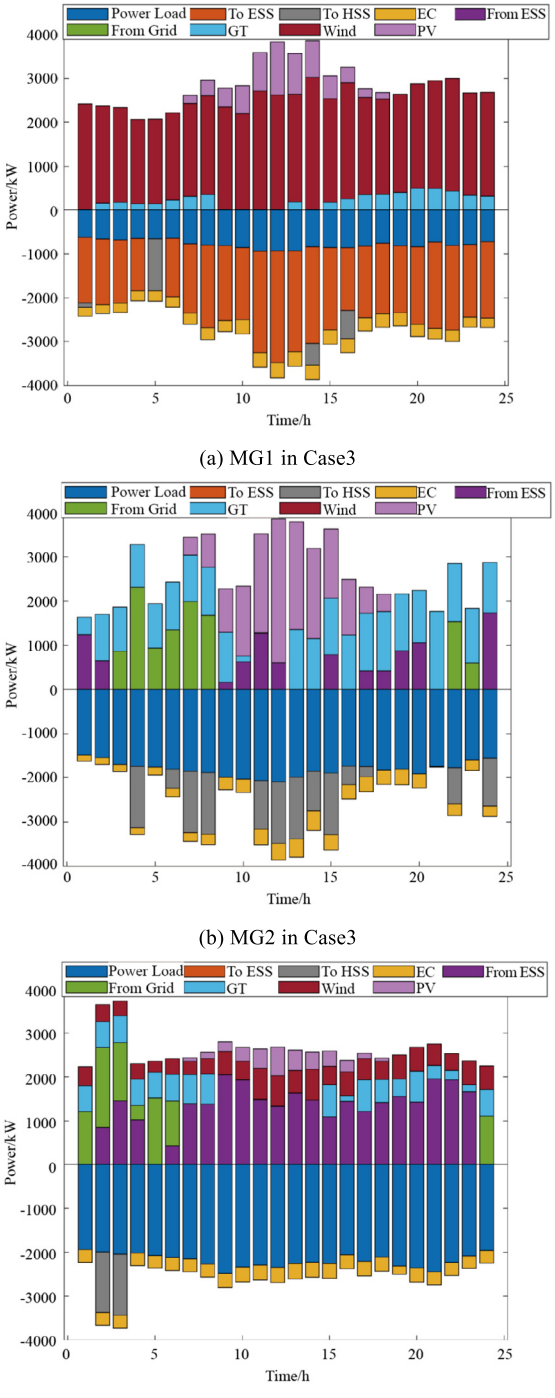


(a) MG1 in Case3

(b) MG2 in Case3

(c)MG3 in Case3

Fig. 6. Optimization of the energy interaction for microgrids on a typical spring day in Case 3.

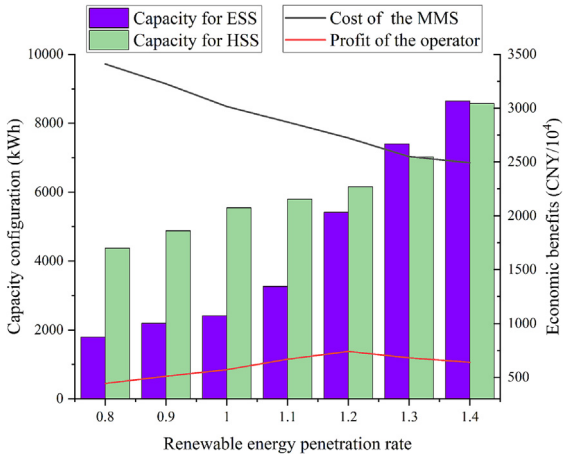


Fig. 7. Sensitivity analysis of renewable energy penetration.

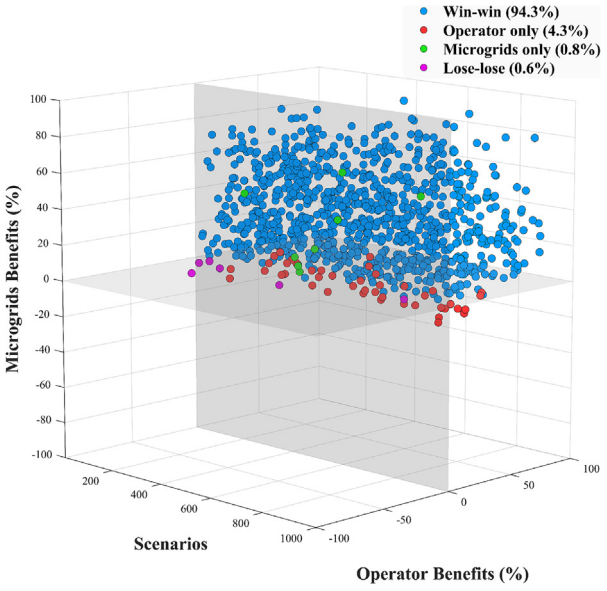


Fig. 8. Comparison of economic benefits between Case 3 and Case 2 across the 1000 generated scenarios.

## 5 Conclusion

For the CCHP MMS with hydrogen energy demand, this paper proposes a bi-level optimization model incorporating shared hybrid electric-hydrogen energy storage services. The upper-level model optimizes the life-cycle capacity configuration of HESS, while the lower-level model focuses on the operational optimization of the MMS, integrating cooling, heating, electricity, and hydrogen energy. By applying the KKT conditions, the lower-level model is transformed into constraints for the upper-level model. Subsequently, the Big-M method linearizes nonlinear components, converting the problem into a MILP model. Case studies validate the economic feasibility and reliability of the proposed scheme, yielding the following key findings:

1) The proposed scheme enables users to access more flexible energy trading options and lower-cost energy procurement channels. The MMS achieves a 20.15% reduction in annual operating costs while increasing the renewable energy utilization rate to 100%.
2) The payback periods for ESS, P2G devices, and hydrogen storage tanks are 1.64 years, 4.74 years, and 7.20 years, respectively–all shorter than their expected service lives. The overall payback period for HESS is only 3.02 years, demonstrating significant profit potential for operators.
3) Integrated HSS-ESS services, capable of meeting diverse energy demands for CCHP microgrid users, demonstrate significant potential in future applications featuring high renewable energy penetration and multi-energy coupling.

## CRediT authorship contribution statement

**Lu Li:** Writing – original draft, Methodology. **Xulong Zhou:** Software. **Shilong Chen:** Supervision. **Guihong Bi:** Data curation. **Zeliang Zhu:** Validation. **Yurui Fan:** Formal analysis, Conceptualization.

### Declaration of competing interest

The authors declare that they have no known competing financial interests or personal relationships that could have appeared to influence the work reported in this paper.

## Appendix A

The Lagrangian function is constructed and presented in Eq. (A1).

$\lambda_{1,r,t,m}$,$\lambda_{2,r,t,m}$,$\lambda_{3r,t,m}$,$\lambda_{4,r,t,m}$,$\lambda_{5,r,t,m}$,$\lambda_{6,r,t,m}$,$\lambda_{7,r,t,m}$ and $\lambda_{8,r,t,m}$ are Lagrangian multipliers corresponding to equality constraints.$u^{\min}_{1,r,t,m}$,$u^{\max}_{1,r,t,m}$,$u^{\min}_{2,r,t,m}$,$u^{\max}_{2,r,t,m}$,$u^{\min}_{3,r,t,m}$,$u^{\max}_{3,r,t,m}$,$u^{\min}_{4,r,t,m}$,$u^{\max}_{4,r,t,m}$,-$u^{\min}_{5,r,t,m}$,$u^{\max}_{5,r,t,m}$,$u^{\min}_{6,r,t,m}$,$u^{\max}_{6,r,t,m}$,$u^{\min}_{7,r,t,m}$,$u^{\max}_{7,r,t,m}$,$u^{\min}_{8,r,t,m}$,$u^{\max}_{8,r,t,m}$,$u^{\max}_{9,r,t,m}$,-$u^{\min}_{10,r,t,m}$,$u^{\max}_{10,r,t,m}$,$u^{\max}_{11,r,t,m}$ and $u^{\min}_{11,r,t,m}$ are Lagrangian multipliers for inequality constraints.

Firstly, Lagrangian multipliers are introduced corresponding to the equational and non-equational constraints respectively. Then use the complementary slackness condition of KKT to construct the Lagrangian function (A1), the lower model can be reformulated as a supplementary constraint on the upper model. The obtained single-level mixed-integer nonlinear model is shown in equations. (A2)−(A40).

$$
\begin{aligned}
L = \sum_{m=1}^{M}\sum_{r=1}^{N}\sum_{t=1}^{N_T} t\left[\begin{array}{c}\varphi_{\mathrm{grid}}(t)P_{\mathrm{grid},m,r}(t)+\frac{\varphi_{\mathrm{gas}}P_{\mathrm{GT},m,r}(t)}{\eta_{\mathrm{GT}}L_{\mathrm{GT}}}+\frac{\varphi_{\mathrm{gas}}Q_{\mathrm{GB},m,r}(t)}{\eta_{\mathrm{GT}}L_{\mathrm{GT}}}+\varphi_{\mathrm{d}}^{\mathrm{sale}}(t)P_{\mathrm{ess,b},m,r}(t)+\varphi(t)P_{\mathrm{ess,b},m,r}(t)+\varphi(t)P_{\mathrm{ess,s},m,r}(t)\\ +\varphi(t)P_{\mathrm{hss,s},m,r}(t)+\varphi_{\mathrm{h}}^{\mathrm{sale}}(t)P_{\mathrm{hss,b},m,r}(t)-\varphi_{\mathrm{d}}^{\mathrm{buy}}(t)P_{\mathrm{ess,s},m,r}(t)-\varphi_{\mathrm{h}}^{\mathrm{buy}}(t)P_{\mathrm{hss,s},m,r}(t)\end{array}\right]\\
\lambda_{1,r,t,m}\left[P_{\mathrm{GT},m,r}(t)+P_{\mathrm{WT},m,r}(t)+P_{\mathrm{PV},m,r}(t)+P_{\mathrm{grid},m,r}(t)+P_{\mathrm{ess,b},m,r}(t)-P_{\mathrm{ess,s},m,r}(t)-P_{\mathrm{EC},m,r}(t)-P_{\mathrm{load},m,r}(t)-P_{\mathrm{hss,s},m,r}(t)\right]+\\
\lambda_{2,r,t,m}\left[P_{\mathrm{EC},m,r}(t)\eta_{\mathrm{EC}}+Q_{\mathrm{AC},m,r}(t)-P_{\mathrm{cool},m,r}(t)\right]+\lambda_{3,r,t,m}\left[Q_{\mathrm{GB},m,r}(t)+P_{\mathrm{HX},m,r}(t)-P_{\mathrm{heat},m,r}(t)\right]+\\
\lambda_{4,r,t,m}\left[P_{\mathrm{HX},m,r}(t)/\eta_{\mathrm{HX}}-P_{\mathrm{GT},m,r}(t)\gamma_{\mathrm{GT}}\eta_{\mathrm{WH}}+Q_{\mathrm{AC},m,r}(t)/\eta_{\mathrm{AC}}\right]+\lambda_{r,5,t,m}\left\{\sum_{i=1}^{N}\left[P_{\mathrm{ess,b},m,r}(t)-P_{\mathrm{ess,s},m,r}(t)\right]-P_{\mathrm{ess,rel},m}(t)+P_{\mathrm{ess,abs},m}(t)\right\}+\\
\lambda_{6,r,t,m}\left\{\sum_{i=1}^{N}\left[P_{\mathrm{hss,s},m,r}(t)\right]-P_{\mathrm{hss,abs},m}(t)\right\}+\lambda_{7,r,t,m}\left\{\sum_{i=1}^{N}\left[P_{\mathrm{hss,b},m,r}(t)\right]-P_{\mathrm{hss,rel},m}(t)+P_{\mathrm{hss,q},m}\right\}+\lambda_{8,r,t,m}\left\{P_{\mathrm{hss,b},m,r}(t)-P_{\mathrm{hload},m,r}(t)\right\} \qquad \text{(A1)}\\
+u_{1,r,t,m}^{\min}\left[P_{\mathrm{GT}}^{\min}-P_{\mathrm{GT},m,r}(t)\right]+u_{1,r,t,m}^{\max}\left[P_{\mathrm{GT},m,r}(t)-P_{\mathrm{GT}}^{\max}\right]++u_{2,r,t,m}^{\min}\left[Q_{\mathrm{AC}}^{\min}-Q_{\mathrm{AC},m,r}(t)\right]+u_{2,r,t,m}^{\max}\left[Q_{\mathrm{AC},m,r}(t)-Q_{\mathrm{AC}}^{\max}\right]\\
+u_{3,r,t,m}^{\min}\left[P_{\mathrm{EC}}^{\min}-P_{\mathrm{EC},m,r}(t)\right]+u_{3,r,t,m}^{\max}\left[P_{\mathrm{EC},m,r}(t)-P_{\mathrm{EC}}^{\max}\right]+u_{4,r,t,m}^{\min}\left[Q_{\mathrm{GB}}^{\min}-Q_{\mathrm{GB},m,r}(t)\right]+u_{4,r,t,m}^{\max}\left[Q_{\mathrm{GB},m,r}(t)-Q_{\mathrm{GB}}^{\max}\right]\\
+u_{5,r,t,m}^{\min}\left[P_{\mathrm{HX}}^{\min}-P_{\mathrm{HX},m,r}(t)\right]+u_{5,r,t,m}^{\max}\left[P_{\mathrm{HX},m,r}(t)-P_{\mathrm{HX}}^{\max}\right]-u_{6,r,t,m}^{\min}P_{\mathrm{grid},m,r}(t)+u_{6,r,t,m}^{\max}\left[P_{\mathrm{grid},m,r}(t)-P_{\mathrm{grid,\ mg}}^{\max}\right]-u_{7,r,t,m}^{\min}P_{\mathrm{ess,s},m,r}(t)\\
+u_{7,r,t,m}^{\max}\left[P_{\mathrm{ess,s},m,r}(t)-P_{\mathrm{ess,mg}}^{\max}U_{\mathrm{s},m,r}(t)\right]-u_{8,r,t,m}^{\min}P_{\mathrm{ess,b},m,r}(t)+u_{8,r,t,m}^{\max}\left[P_{\mathrm{ess,b},m,r}(t)-P_{\mathrm{ess,mg}}^{\max}U_{\mathrm{b},m,r}(t)\right]+u_{9,r,t,m}^{\max}\left[U_{\mathrm{s},m,r}(t)+U_{\mathrm{b},m,r}(t)-1\right]\\
-u_{10,r,t,m}^{\min}P_{\mathrm{hss,s},m,r}(t)+u_{10,r,t,m}^{\max}\left[P_{\mathrm{hss,s},m,r}(t)-P_{\mathrm{hss,mg}}^{\max}\right]-u_{11,r,t,m}^{\min}P_{\mathrm{hss,b},m,r}(t)+u_{11,r,t,m}^{\max}\left[P_{\mathrm{hss,b},m,r}(t)-P_{\mathrm{hss,hmg}}^{\max}\right]
$$

$$
\begin{aligned}
&\min C=\sum_{m=1}^{M}[T_m(C_{\mathrm{inv},m,\mathrm{ess}}+C_{\mathrm{inv},m,\mathrm{hss}}+C_{\mathrm{ess},m,\mathrm{s}}+C_{\mathrm{hss},m,\mathrm{s}}+\\
&\quad C_{\mathrm{trans},m}-C_{\mathrm{serve},m}-C_{\mathrm{ess},m,\mathrm{b}}-C_{\mathrm{hss},m,\mathrm{b}}-C_{\mathrm{hss},m,\mathrm{q}})] && \text{(A2)}\\
&E_{\mathrm{ess}}^{\max}=\delta_{\mathrm{ess}}P_{\mathrm{ess}}^{\max} && \text{(A3)}\\
&E_{\mathrm{ess},m}(t)=\Delta t\cdot[\eta_{\mathrm{ess}}^{\mathrm{abs}}P_{\mathrm{ess,abs},m}(t)-\tfrac{1}{\eta_{\mathrm{ess}}^{\mathrm{rel}}}P_{\mathrm{ess,rel},m}(t)]+E_{\mathrm{ess},m}(t-1)\\
&\quad 10\%E_{\mathrm{ess},m}^{\max}\le E_{\mathrm{ess}}(t)\le 90\%E_{\mathrm{ess},m}^{\max}\\
&\quad 0\le P_{\mathrm{ess,abs},m}(t)\le P_{\mathrm{ess},m}^{\max}U_{\mathrm{abs}}(t)\\
&\quad 0\le P_{\mathrm{ess,rel},m}(t)\le P_{\mathrm{ess},m}^{\max}U_{\mathrm{rel}}\ (t) && \text{(A4)}\\
&\quad U_{\mathrm{abs}}\ (t)+U_{\mathrm{rel}}\ (t)\le 1\\
&\quad U_{\mathrm{abs}}\ (t)\in\{0,1\},U_{\mathrm{rel}}\ (t)\in\{0,1\}\\
&E_{\mathrm{tan}\,k}^{\max}=\delta_{\mathrm{hss}}P_{\mathrm{p2g}}^{\max} && \text{(A5)}\\
&E_{\mathrm{tank},m}(t)=\Delta t\cdot[\eta_{\mathrm{hss},m}^{\mathrm{abs}}P_{\mathrm{hss,abs},m}(t)-\tfrac{P_{\mathrm{hss,rel},m}(t)}{\eta_{\mathrm{hss}}^{\mathrm{rel}}}]+E_{\mathrm{tan}\,k,m}(t-1)\\
&\quad 10\%E_{\mathrm{tan}\,k}^{\max}\le E_{\mathrm{tan}\,k,m}(t)\le 90\%E_{\mathrm{tan}\,k}^{\max}\\
&\quad 0\le P_{\mathrm{hss,abs},m}(t)\le P_{\mathrm{p2g}}^{\max} && \text{(A6)}\\
&\quad 0\le P_{\mathrm{hss,rel},m}(t)\le P_{\mathrm{trans}}^{\max}\\
&0\le P_{\mathrm{hss,q},m}(t)\le P_{\mathrm{hload},m}(t) && \text{(A7)}\\
&T_m\varphi_{\mathrm{gas}}/(\eta_{\mathrm{GT}}L_{\mathrm{NG}})-\lambda_{4,r,t,m}\gamma_{\mathrm{GT}}\eta_{\mathrm{WH}}+\lambda_{1,r,t,m}+u_{1,r,t,m}^{\max}\\
&\quad -u_{1,r,t,m}^{\min}=0 && \text{(A8)}\\
&T_m\varphi_{\mathrm{grid}}(t)+\lambda_{1,r,t,m}+u_{6,r,t,m}^{\max}-u_{6,r,t,m}^{\min}=0 && \text{(A9)}\\
&T_m[\varphi_{\mathrm{d}}^{\mathrm{sale}}(t)+\varphi(t)]+\lambda_{1,r,t,m}+u_{8,r,t,m}^{\max}-u_{8,r,t,m}^{\min}+\\
&\quad \lambda_{5,r,t,m}=0 && \text{(A10)}\\
&T_m[-\varphi_{\mathrm{d}}^{\mathrm{buy}}(t)+\varphi(t)]-\lambda_{1,r,t,m}+u_{7,r,t,m}^{\max}-u_{7,r,t,m}^{\min}\\
&\quad -\lambda_{5,r,t,m}=0 && \text{(A11)}\\
&-\lambda_{1,r,t,m}+\lambda_{2,r,t,m}\eta_{\mathrm{EC}}+u_{3,r,t,m}^{\max}-u_{3,r,t,m}^{\min}=0 && \text{(A12)}\\
&\lambda_{3,r,t,m}+\lambda_{4,r,t,m}/\eta_{\mathrm{HX}}+u_{5,r,t,m}^{\max}-u_{5,r,t,m}^{\min}=0 && \text{(A13)}\\
&T_m\varphi_{\mathrm{gas}}/(\eta_{\mathrm{GB}}L_{\mathrm{NG}})+\lambda_{3,r,t,m}+u_{4,r,t,m}^{\max}-u_{4,r,t,m}^{\min}=0 && \text{(A14)}\\
&\lambda_{2,r,t,m}+\lambda_{4,r,t,m}/\eta_{\mathrm{AC}}+u_{2,r,t,m}^{\max}-u_{2,r,t,m}^{\min}=0 && \text{(A15)}\\
&-u_{8,r,t,m}^{\max}P_{\mathrm{ess,mg}}^{\max}+u_{9,r,t,m}^{\max}=0 && \text{(A16)}\\
&-u_{7,r,t,m}^{\max}P_{\mathrm{ess,mg}}^{\max}+u_{9,r,t,m}^{\max}=0 && \text{(A17)}\\
&T_m[-\varphi_{\mathrm{h}}^{\mathrm{buy}}(t)+\varphi(t)]-\lambda_{1,r,t,m}+\lambda_{7,r,t,m}-u_{10,r,t,m}^{\min}+\\
&\quad u_{10,r,t,m}^{\max}=0 && \text{(A18)}\\
&T_m\varphi_{\mathrm{h}}^{\mathrm{sell}}(t)+\lambda_{6,r,t,m}+\lambda_{8,r,t,m}-u_{11,r,t,m}^{\min}+u_{11,r,t,m}^{\max}=0 && \text{(A19)}\\
&0\le u_{1,r,t,m}^{\min}\perp\left(P_{\mathrm{GT},m,r}(t)-P_{\mathrm{GT}}^{\min}\right)\ge 0 && \text{(A20)}\\
&0\le u_{1,r,t,m}^{\max}\perp\left(P_{\mathrm{GT}}^{\max}-P_{\mathrm{GT},m,r}(t)\right)\ge 0 && \text{(A21)}
\end{aligned}
$$

$$0 \le u^{\min}_{2,r,t,m} \perp \left(Q_{\mathrm{AC},m,r}(t) - Q^{\min}_{\mathrm{AC}}\right) \ge 0 \tag{A22}$$

$$0 \le u^{\max}_{2,r,t,m} \perp \left(Q^{\max}_{\mathrm{AC}} - Q_{\mathrm{AC},m,r}(t)\right) \ge 0 \tag{A23}$$

$$0 \le u^{\min}_{3,r,t,m} \perp \left(P_{\mathrm{EC},m,r}(t) - P^{\min}_{\mathrm{EC}}\right) \ge 0 \tag{A24}$$

$$0 \le u^{\max}_{3,r,t,m} \perp \left(P^{\max}_{\mathrm{EC}} - P_{\mathrm{EC},m,r}(t)\right) \ge 0 \tag{A25}$$

$$0 \le u^{\min}_{4,r,t,m} \perp \left(Q_{\mathrm{GB},m,r}(t) - Q^{\min}_{\mathrm{GB}}\right) \ge 0 \tag{A26}$$

$$0 \le u^{\max}_{4,r,t,m} \perp \left(Q^{\max}_{\mathrm{GB}} - Q_{\mathrm{GB},m,r}(t)\right) \ge 0 \tag{A27}$$

$$0 \le u^{\min}_{5,r,t,m} \perp \left(P_{\mathrm{HX},m,r}(t) - P^{\min}_{\mathrm{HX}}\right) \ge 0 \tag{A28}$$

$$0 \le u^{\max}_{5,r,t,m} \perp \left(P^{\max}_{\mathrm{HX}} - P_{\mathrm{HX},m,r}(t)\right) \ge 0 \tag{A29}$$

$$0 \le u^{\min}_{6,r,t,m} \perp P_{\mathrm{grid},m,r}(t) \ge 0 \tag{A30}$$

$$0 \le u^{\max}_{6,r,t,m} \perp \left(P^{\max}_{\mathrm{grid,mg}} - P_{\mathrm{grid},m,r}(t)\right) \ge 0 \tag{A31}$$

$$0 \le u^{\min}_{7,r,t,m} \perp P_{\mathrm{ess,s},m,r}(t) \ge 0 \tag{A32}$$

$$0 \le u^{\max}_{7,r,t,m} \perp \begin{pmatrix} P^{\max}_{\mathrm{ess,mg}} \cdot U_{\mathrm{s},m,r}(t) \\ -P_{\mathrm{ess,s},m,r}(t) \end{pmatrix} \ge 0 \tag{A33}$$

$$0 \le u^{\min}_{8,r,t,m} \perp P_{\mathrm{ess,b},m,r}(t) \ge 0 \tag{A34}$$

$$0 \le u^{\max}_{8,r,t,m} \perp \begin{pmatrix} P^{\max}_{\mathrm{ess,mg}} \cdot U_{\mathrm{b},m,r}(t) \\ -P_{\mathrm{ess,b},m,r}(t) \end{pmatrix} \ge 0 \tag{A35}$$

$$0 \le u^{\max}_{9,r,t,m} \perp \left(1 - U_{\mathrm{s},m,r}(t) - U_{\mathrm{b},m,r}(t)\right) \ge 0 \tag{A36}$$

$$0 \le u^{\min}_{10,r,t,m} \perp P_{\mathrm{hss,s},m,r}(t) \ge 0 \tag{A37}$$

$$0 \le u^{\max}_{10,r,t,m} \perp \left(P^{\max}_{\mathrm{hss,mg}} - P_{\mathrm{hss,s},m,r}(t)\right) \ge 0 \tag{A38}$$

$$0 \le u^{\min}_{11,r,t,m} \perp P_{\mathrm{hss,b},m,r}(t) \ge 0 \tag{A39}$$

$$0 \le u^{\max}_{11,r,t,m} \perp \left(P^{\max}_{\mathrm{hss,hmg}} - P_{\mathrm{hss,b},m,r}(t)\right) \ge 0 \tag{A40}$$

The formula "$0 \le a \perp b \ge 0$" indicates $ab = 0$, and $a \ge 0$, $b \ge 0$. The Big-M method is then employed to linearize the non-linear constraints (A4), (A6) and (A20)–(A40). For example, constraint (A4) is converted to constraint (A41) and constraint (A20) is converted to constraints (A42) and (A43). The transformation of constraints (A6) is like that of constraint (A4), and the transformation of constraints (A21)–(A40) is like that of constraint (A20).

$$\begin{gathered} E_{\mathrm{ess},m}(t) = E_{\mathrm{ess},m}(t-1) + \left[\eta^{\mathrm{abs}}_{\mathrm{ess}} P_{\mathrm{ess,abs},m}(t) - \frac{1}{\eta^{\mathrm{rel}}_{\mathrm{ess}}} P_{\mathrm{ess,rel},m}(t)\right]\Delta t \\ 10\% E^{\max}_{\mathrm{ess},m} \le E_{\mathrm{ess},m}(t) \le 90\% E^{\max}_{\mathrm{ess},m} \\ 0 \le P_{\mathrm{ess,abs},m}(t) \le P^{\max}_{\mathrm{ess},m} \\ 0 \le P_{\mathrm{ess,abs},m}(t) \le M U_{\mathrm{abs}}(t) \\ 0 \le P_{\mathrm{ess,rel},m}(t) \le P^{\max}_{\mathrm{ess},m} \\ 0 \le P_{\mathrm{ess,rel},m}(t) \le M U_{\mathrm{rel}}\ (t) \\ U_{\mathrm{abs}}\ (t) + U_{\mathrm{rel}}\ (t) \le 1 \\ U_{\mathrm{abs}}\ (t) \in \{0,1\}, U_{\mathrm{rel}}\ (t) \in \{0,1\} \end{gathered} \tag{A41}$$

$$0 \le u^{\min}_{1,r,t,m} \le M^{\min}_{u} v^{\min}_{u,r,t,m} \tag{A42}$$

$$0 \le P_{\mathrm{GT},m,r}(t) - P^{\min}_{\mathrm{GT}} \le M^{\min}_{u}\left(1 - v^{\min}_{u,r,t,m}\right) \tag{A43}$$

In above equations, $M$ and $M^{\min}_{u}$ represent a large constants taken as $10^5$;$v^{\min}_{u,r,t}$ represents a binary variable.

## Appendix B

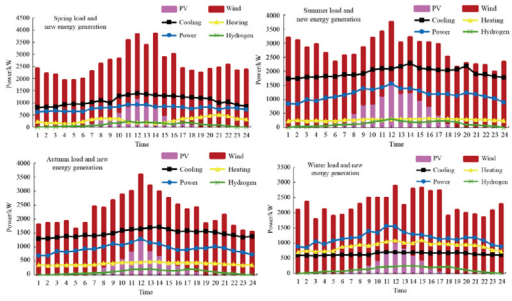


(a) The cooling, heating, power, hydrogen load, and PV wind forecast in MG1

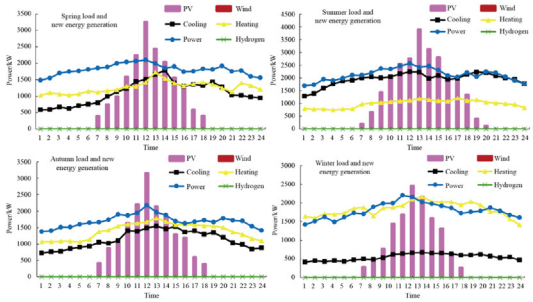


(b) The cooling, heating, power, hydrogen load, and PV wind forecast in MG2

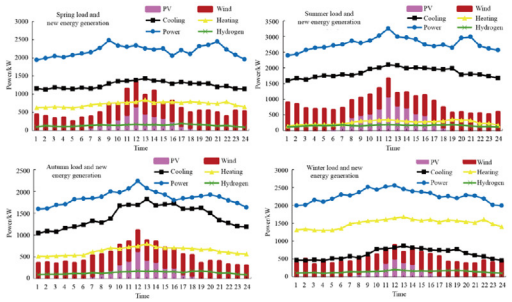


(c) The cooling, heating, power, hydrogen load, and PV wind forecast in MG3

Fig. B1. Clustered data of microgrids

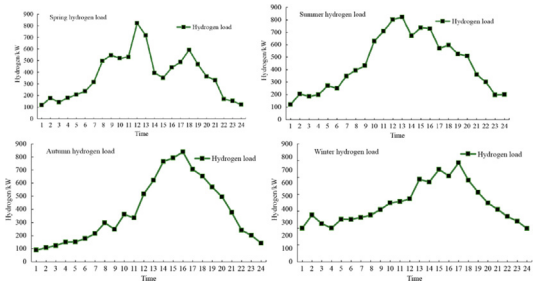


Fig. B2. Clustered data of the outside energy market

## Appendix C

**Table C1**
**Equipment-related parameters of microgrids.**

| Parameters | Value | Parameters | Value |
|---|---|---|---|
| $\eta_{GT}$ | 0.3 | $P_{EC}^{max}$ | 4000 kW |
| $\gamma_{GT}$ | 1.47 | $\eta_{HX}$ | 0.9 |
| $P_{GT}^{max}$ | 3000 kW | $P_{HX}^{max}$ | 4000 kW |
| $\eta_{WH}$ | 0.8 | $\eta_{GB}$ | 0.9 |
| $\eta_{AC}$ | 1.2 | $Q_{GB}^{max}$ | 4000 kW |
| $Q_{AC}^{max}$ | 4000 kW | $P_{ess,mg}^{max}$ | 4000 kW |
| $\eta_{EC}$ | 4 | $\eta_{ess}^{abs}$ | 0.95 |
| $P_{hss,mg}^{max}$ | 4000 kW | $\eta_{ess}^{rel}$ | 0.95 |
| $\eta_{h_2}^{trans}$ | 39.72 kWh/kg | $\eta_{hss}^{abs}$ | 0.8 |
| $P_{hss,hmg}^{max}$ | 1000 kW | $\eta_{hss}^{rel}$ | 0.99 |
| $P_{trans}^{max}$ | 4000 kW | | |

## References


[1] S. Raza et al., Advances in technology and utilization of natural resources for achieving carbon neutrality and a sustainable solution to neutral environment, Environ. Res. 220 (2023) 115135.
[2] J. Yao, H.D. Han, Y. Yang, Y.M. Song, G.H. Li, A review of recent progress of carbon capture, utilization, and storage (CCUS) in China, Appl. Sci.-Basel 13 (2) (2023) 1169.
[3] C.W. Lu, K. Wang, Natural resource conservation outpaces and climate change: Roles of reforestation, mineral extraction, and natural resources depletion, Res. Policy 86 (2023) 104159.
[4] X. Li, C.J. Raorane, C. Xia, Y. Wu, T.K.N. Tran, T. Khademi, Latest approaches on green hydrogen as a potential source of renewable energy towards sustainable energy: Spotlighting of recent innovations, challenges, and future insights, Fuel 334 (2023).
[5] M.-T. Huang, P.-M. Zhai, Achieving Paris agreement temperature goals requires carbon neutrality by middle century with far-reaching transitions in the whole society, Adv. Clim. Chang. Res. 12 (2) (2021) 281–286.
[6] Y. Zhou, J. Wang, Y. Liu, R. Yan, Y. Ma, Incorporating deep learning of load predictions to enhance the optimal active energy management of combined cooling, heating and power system, Energy 233 (2021).
[7] Y. Li, F. Zhang, Y. Li, Y. Wang, An improved two-stage robust optimization model for CCHP-P2G microgrid system considering multi-energy operation under wind power outputs uncertainties, Energy 223 (2021).
[8] X. Yang, K. Liu, Z. Leng, T. Liu, L. Zhang, L. Mei, Multi-dimensions analysis of solar hybrid CCHP systems with redundant design, Energy 253 (2022).
[9] W. Guo, Q. Wang, H. Liu, W.A. Desire, Multi-energy collaborative optimization of park integrated energy system considering carbon emission and demand response, Energy Rep. 9 (2023) 3683–3694.
[10] Z. Siqin, D. Niu, X. Wang, H. Zhen, M. Li, J. Wang, A two-stage distributionally robust optimization model for P2G-CCHP microgrid considering uncertainty and carbon emission, Energy 260 (2022).
[11] Z. Cheng, D. Jia, Z. Li, J. Si, S. Xu, Multi-time scale dynamic robust optimal scheduling of CCHP microgrid based on rolling optimization, Int. J. Electr. Power Energy Syst. 139 (2022).
[12] Y. Li, F. Yao, S. Zhang, Y. Liu, S. Miao, An optimal dispatch model of adiabatic compressed air energy storage system considering its temperature dynamic behavior for combined cooling, heating and power microgrid dispatch, J. Storage Mater. 51 (2022).
[13] H. Chen et al., Grid resilience with high renewable penetration: A PJM approach, IEEE Trans. Sustain. Energ. 14 (2) (2023) 1169–1177.
[14] B. Modu, M.P. Abdullah, A.L. Bukar, M.F. Hamza, A systematic review of hybrid renewable energy systems with hydrogen storage: sizing, optimization, and energy management strategy, Int. J. Hydrogen Energy 48 (97) (2023) 38354–38373.
[15] B. Zheng, W. Wei, Y. Chen, Q. Wu, S. Mei, A peer-to-peer energy trading market embedded with residential shared energy storage units, Appl. Energy 308 (2022).
[16] N. Liu, M. Cheng, X. Yu, J. Zhong, J. Lei, Energy-sharing provider for PV prosumer clusters: a hybrid approach using stochastic programming and stackelberg game, IEEE Trans. Ind. Electron. 65 (8) (2018) 6740–6750.
[17] J. Liu, N. Zhang, C. Kang, D.S. Kirschen, Q. Xia, Decision-making models for the participants in cloud energy storage, IEEE Trans. Smart Grid 9 (6) (2018) 5512–5521.
[18] T. Zhang, Y. Ma, Y. Wu, L. Yi, Optimization configuration and application value assessment modeling of hybrid energy storage in the new power system with multi-flexible resources coupling, J. Storage Mater. 62 (2023).
[19] Q. Hassan, A.Z. Sameen, H.M. Salman, M. Jaszczur, A.K. Al-Jiboory, Hydrogen energy future: Advancements in storage technologies and implications for sustainability, J. Storage Mater. 72 (2023).
[20] T. Zhang, J. Uratani, Y. Huang, L. Xu, S. Griffiths, Y. Ding, Hydrogen liquefaction and storage: recent progress and perspectives, Renew. Sustain. Energy Rev. 176 (2023).
[21] J. Li, Y. Xiao, S. Lu, Optimal configuration of multi microgrid electric hydrogen hybrid energy storage capacity based on distributed robustness, J. Storage Mater. 76 (2024).
[22] H. Deng et al., Optimization of configurations and scheduling of shared hybrid electric hydrogen energy storages supporting to multi-microgrid system, J. Storage Mater. 74 (2023).
[23] Q. Li, X. Xiao, Y. Pu, S. Luo, H. Liu, W. Chen, Hierarchical optimal scheduling method for regional integrated energy systems considering electricity-hydrogen shared energy, Appl. Energy 349 (2023).
[24] Y.L. Xie et al., Shared energy storage configuration in distribution networks: A multi-agent tri-level programming approach, Appl. Energy 372 (2024) 123771.
[25] L. Li, et al., "A Review of Research on Shared Energy Storage Operation Models and Pricing Strategies," in: Presented at the 2024 3RD Asian conference on Frontiers of Power and Energy, ACFPE 2024, 2024.
[26] S. Wu, J. Liu, Q. Zhou, C. Wang, Z. Chen, Optimal economic scheduling for multi-microgrid system with combined cooling, heating and power considering service of energy storage station, Automat. Electr. Power Syst. 43 (10) (2019) 10–18.
[27] Y. Xie, Y. Luo, Z. Li, Z. Xu, L. Li, K. Yang, Optimal allocation of shared energy storage considering the economic consumption of microgrid new energy, High Volt. Eng. 48 (11) (2022) 4403–4412.
[28] F.Q. Xu, X.P. Li, C.H. Jin, Optimal capacity configuration and dynamic pricing strategy of a shared hybrid hydrogen energy storage system for integrated energy system alliance: a bi-level, Int. J. Hydrogen Energy 69 (2024) 331–346.
[29] S. Wu, Q. Li, J. Liu, Q. Zhou, C. Wang, Bi-level optimal configuration for combined cooling heating and power multi-

microgrids based on energy storage station service, Power Syst. Technol. 45 (10) (2021) 3822–3832.
[30] A. Acakpovi, P. Adjei, N. Nwulu, N.Y. Asabere, P.-F. Pai, Optimal hybrid renewable energy system: a comparative study of wind/hydrogen/fuel-cell and wind/battery storage, J. Electr. Comput. Eng. 2020 (2020) 1–15.

**Lu Li** received the Ph.D. degree at North China Electric Power University, Hebei, China, in 2015. Currently, she is an Associate Professor at the Faculty of Electrical Engineering, Kunming University of Science and Technology, Kunming, China. Her research interests include electricity markets and energy economics.